

pubs.acs.org/Macromolecules Article

# Synthesis of High Etch Contrast Poly(3-hydroxystyrene)-Based Triblock Copolymers and Self-Assembly of Sub-5 nm Features

Jian Sun, Changyeon Lee, Chinedum O. Osuji, and Padma Gopalan\*



Cite This: Macromolecules 2021, 54, 9542-9550



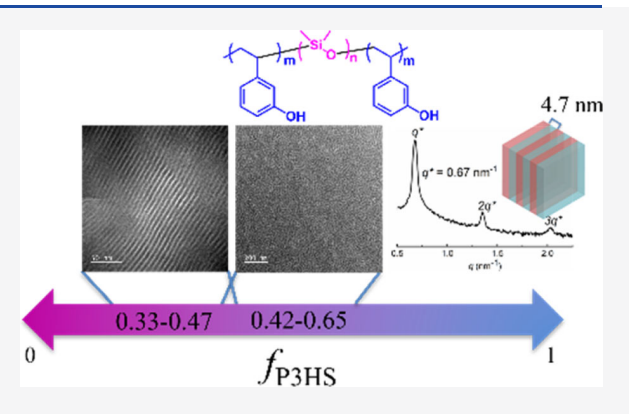
**ACCESS** 

III Metrics & More

Article Recommendations

s Supporting Information

ABSTRACT: We demonstrate the successful synthesis of a series of poly(3-hydroxystyrene)-block-poly(dimethylsiloxane)-block-poly(3-hydroxystyrene) (P3HS-b-PDMS-b-P3HS) triblock copolymers by atom transfer radical polymerization (ATRP). This system is a promising candidate for pattern transfer of single-digit nanometer features, due to its intrinsic high etch contrast, etch versatility, and the triblock architecture. Hydroxy-terminated PDMS polymers were directly functionalized to initiate the ATRP of an acetal-protected 3-hydroxystyrene monomer. The resulting triblocks have dispersity ranging from 1.10 to 1.26, and the synthesis provides robust control over molecular weights and volume fractions. The large chemical incompatibility between the blocks enabled the formation of ordered structures at low molecular weights, which yielded lamellar periodicities as small as 9.3 nm. This triblock hence permits access to sub-5 nm



feature sizes. The phase diagram is asymmetric, with lamellar morphologies observed at lower volume fractions of the P3HS block, relative to the diblocks. This asymmetry is ascribed to the dispersity of the middle block relative to the end blocks.

#### **■ INTRODUCTION**

Block copolymer (BCP) self-assembly has been widely used in the past two decades to generate nanoscale periodic patterns over large areas. 1-3 Phase separation of a BCP is dictated by the degree of polymerization (N), the volume fraction of each block  $(f_A = 1 - f_B)$ , and the Flory–Huggins interaction parameter  $(\chi)$ .<sup>4–7</sup> The product of  $\chi N$  gives a measure of the segregation strength of a BCP. For symmetrical BCPs, the value of  $\chi N$  must be above 10.5 in order to self-assemble.<sup>8</sup> In principle, the resultant lamellar periodicity  $(L_0)$  scales as  $L_0 \approx$  $\chi^{1/6}$   $N^{\alpha}$  where  $\alpha = 2/3$  and  $\alpha = 1/2$  for strong and weakly segregated systems, respectively. 9,10 Many recent studies of BCPs 11-18 have been motivated by their potential use in microelectronics. Specifically, directed self-assembly (DSA) of BCPs is one of the many potential solutions for the limitations of the current lithography techniques, as sub-10 nm feature sizes over large areas can be achieved in a scalable and costeffective manner to meet the needs of microelectronic industry. 18-21

Thus far, polystyrene-*b*-poly(methyl methacrylate) (PS-*b*-PMMA) has been the material of choice for BCP thin-film self-assembly. <sup>22,23</sup> Due to its relatively small interaction parameter (0.03 at 150 °C), PS-*b*-PMMA is limited to high-fidelity patterning of features larger than 11 nm. <sup>24–26</sup> To achieve single-digit pattern transfer by BCP self-assembly, BCPs that exhibit high  $\chi$  are needed because they allow reduction of the feature sizes while maintaining the segregation strength above the self-assembly threshold. One guideline in designing high- $\chi$ 

BCPs is to increase the incompatibility between the two blocks by increasing the polarity mismatch. This has typically been demonstrated by incorporating highly polar blocks such as poly(hydroxystyrene), <sup>15,27–29</sup> poly(dihydroxystyrene), <sup>16</sup> or poly(glycerol monomethacrylate), <sup>17</sup> with PS as the second block in a diblock architecture. As a result, sub-5 nm features have been demonstrated in these studies.

However, one of the major roadblocks is achieving successful pattern transfer from these high- $\chi$  BCPs due to insufficient etch contrast between the blocks. The required etch contrast at small length scales becomes even more critical for achieving high aspect ratio features. Key studies have focused on poly(dimethylsiloxane) (PDMS) as a highly hydrophobic inorganic block in the BCP, which provides higher etch contrast to achieve sub-10 nm pattern transfer.  $^{30,31}$  Alternatively, etch contrast between the blocks at these small length scales can be increased by sequential infiltration of inorganic elements selectively into one block. For example, sequential infiltration of organometallic precursors selectively into PMMA block has been demonstrated by Elam et al.  $^{32,33}$ 

Received: July 30, 2021 Revised: September 25, 2021 Published: October 13, 2021





The interaction between the organometallic precursors and carbonyl groups in the PMMA domain converts PMMA to oxides such as Al<sub>2</sub>O<sub>3</sub> or TiO<sub>2</sub> without disturbing the BCP morphology. Hence, BCP lamellae or cylinder features can be transformed into oxide nanowires or nanopillars to provide sufficient etch contrast for pattern transfer with high fidelity.<sup>34</sup> Similarly, successful pattern transfer down to a 10 nm length scale has been demonstrated using cylinder-forming poly(4-tert-butylstyrene)-b-poly(2-vinylpyridine) coupled with sequential infiltration of alumina precursors into the poly(2-vinylpyridine) block followed by reactive ion etching.<sup>25</sup>

We recently expanded the library of high-γ BCPs by introducing polyhydroxystyrene (PHS)-based BCPs including poly(3-hydroxystyrene)-b-poly(dimethylsiloxane) (P3HS-b-PDMS). 15,27-29 Protected monomer 3-(2tetrahydropyranyloxy)styrene (3OTHPSt) was effectively polymerized by living anionic polymerization to synthesize phenol-containing BCPs. Acetal deprotection requires mild acidic conditions, hence allowing for the incorporation of acidsensitive blocks such as PDMS. PDMS as an inorganic segment possesses high hydrophobicity and it can be converted to robust oxides if treated with oxygen plasma to enhance the etch contrast. The interaction parameter of the P3HS-b-PDMS was estimated to be 0.39 at 150  $^{\circ}\text{C}\text{,}$  with a smallest lamellar periodicity of 7.4 nm observed. 15 This new BCP not only exhibits a high etch contrast of 1:15 between PDMS and P3HS under oxygen plasma but also offers etch versatility, as P3HS provides possibilities for further transformations by postfunctionalization reactions.35,36

Compared to diblock copolymers, ABA triblock copolymers offer advantages in thin-film assembly. Both theoretical and experimental studies indicate that linear ABA triblock copolymers have a higher tendency toward forming perpendicular nanostructures. 37-39 When the midblock B has lower surface energy and forms a wetting layer at the air interface, the higher surface energy A end blocks are likely to migrate to the air interface due to the greatly increased end-segment entropy. 40-43 Triblocks have been reported to have a larger processing window in a thin film compared to their analogous diblocks. 44-46 They are known to form smaller features than that of diblocks with similar molecular weights and to potentially self-assemble into even smaller critical dimensions as they exhibit a lower  $(\chi N)_{\rm ODT}$  value at roughly 9.9.  $^{44,47-49}$ The unique bridging conformation in an ordered phase also enhances the ABA triblock mechanical properties significantly.47,50

Here, we report the synthesis of a series of triblock materials, poly(3-hydroxystyrene)-b-poly(dimethylsiloxane)-b-poly(3-hydroxystyrene) (P3HS-b-PDMS-b-P3HS) by atom transfer radical polymerization (ATRP). Brominated PDMS functionalized from hydroxy-terminated PDMS was used as a macroinitiator, and chain extension was achieved by polymerizing the tetrahydropyran-protected hydroxystyrene. A range of triblock compositions was synthesized and characterized by size exclusion chromatography (SEC),  $^1$ H NMR, and  $^{29}$ Si NMR. Bulk self-assembly analyses by small-angle X-ray scattering (SAXS) and transmission electron microscopy (TEM) confirm phase separation into lamellar and cylindrical morphologies. The smallest  $L_0$  achieved by this triblock system was 9.3 nm. We compare the phase separation behavior of the triblocks with the diblock copolymers.

#### EXPERIMENTAL SECTION

**Materials.** Carbinol (hydroxyl)-terminated PDMSs with various molecular weights, here referred to as HO-PDMS-OH for brevity, were obtained from Gelest and used as received. Details of the PDMS starting materials are shown in Figure S1 and Table S1. All solvents and other reagents were purchased from Sigma-Aldrich Chemical Co. (Milwaukee, WI) and used without further purification unless specified. Tetrahydrofuran (THF) and toluene were freshly purified by using solvent towers purchased from VAC. 3OTHPSt was synthesized and purified according to published procedures.<sup>29</sup>

General Procedure for the Synthesis of a PDMS ATRP **Macroinitiator.** To a solution of HO-PDMS-OH (20 g, ~4 mmol) in THF, triethylamine (4.05 g, 40 mmol) was added. The flask was then transferred to an ice bath.  $\alpha$ -Bromoisobutyryl bromide (2.46 mL, 20 mmol) was slowly added to the solution at 0 °C with stirring. The reaction was carried out overnight at room temperature. After completion of the reaction, triethylammonium bromide salt was first removed by filtration, and the solvent was removed by rotary evaporation. The residue was dissolved in dichloromethane (200 mL) followed by washing with saturated sodium bicarbonate solution (200 mL) twice and deionized water once. The organic layer was then collected, dried over anhydrous sodium sulfate, and concentrated by rotary evaporation. The solution was precipitated in methanol and collected by centrifugation. The final product was obtained as transparent oil after removing volatiles under vacuum (yield: 77%). Br-PDMS-Br: <sup>1</sup>H NMR (400 MHz, CDCl<sub>3</sub>) δ: 4.24 (C-H<sub>2</sub>), 3.60 (C-H<sub>2</sub>), 3.37 (C-H<sub>2</sub>), 1.87 (C-H<sub>3</sub>), 1.53 (C-H<sub>2</sub>), 0.46 (C-H<sub>2</sub>), 0.00 (C-

General Procedure for ATRP and Subsequent Dehalogenation of P3OTHPSt-b-PDMS-b-P3OTHPSt. The triblock copolymers were synthesized by conventional Cu(I)-mediated ATRP of 3OTHPSt according to the following general procedure. First, CuBr (3.5 mg, 0.024 mmol), a Br-PDMS-Br macroinitiator (1.22 g, ~0.24 mmol), and 3OTPHSt (5 g, 24.5 mmol) were mixed in toluene (5 mL) and the system was sealed with a rubber septum. The mixture was degassed with Ar bubbling for 30 min. A tris(2-pyridylmethyl)amine (TPMA) ligand (35 mg, 0.12 mmol) was added to the mixture under an Ar atmosphere followed by additional 5 min of degassing. The flask was sealed under an Ar atmosphere and immersed in a preheated oil bath at 70 °C. The polymerization was carried out overnight (approximately 16 h). Then, tributyltin hydride (208 mg, 0.72 mmol) was added and the reaction was further stirred for 3 h at 70 °C. The polymerization solution was diluted with toluene at room temperature and then was precipitated in 300 mL of methanol followed by filtration. The powder was collected and dried under reduced pressure overnight (typical yield: 50%). P3OTHPSt-b-PDMS-b-P3OTHPSt: <sup>1</sup>H NMR (400 MHz, CDCl<sub>3</sub>)  $\delta$ : 7.15–5.92 (Ar-H), 5.42-5.07 (C-H), 3.98-3.65 (C-H), 3.62-3.38 (C-H), 2.20-0.99 (C-H<sub>2</sub> and backbone), 0.06 (C-H<sub>3</sub>).

**Deprotection of P3OTHPSt-***b***-PDMS**-*b***-P3OTHPSt.** P3OTHPSt. P3OTHPSt-*b*-PDMS-*b*-P3OTHPSt (500 mg, ~0.033 mmol) was dissolved in the mixture of THF/ethanol (20 mL/10 mL). One milliliter of conc. Ac. HCl was diluted to 10 mL with deionized water. HCl solution (0.03 mL) was added to the solution and then stirred for 3 h at room temperature. The solution was then concentrated by rotary evaporation and precipitated from water followed by collecting the powder by vacuum filtration and drying under the reduced pressure (yield: 95%). P3HS-*b*-PDMS-*b*-P3HS:  $^{1}$ H NMR (400 MHz, Acetone- $d_6$ ) δ: 8.22–7.65 (O-H), 7.16–5.89 (Ar-H), 2.24–1.17 (backbone), 0.08 (C-H<sub>3</sub>).

**Characterization.** SEC was performed using a Viscotek 2210 system equipped with three Waters columns (HR4, HR 4E, and HR3). THF was used as the eluent with a flow rate of 1 mL/min at 30 °C. The calibration curve for analysis consisted of nine narrow dispersity PS standards with  $M_{\rm n}$  from 1 to 400 kg/mol. TGA was carried out with a TA Instruments Q500 using a heating rate of 10 °C/min under a nitrogen atmosphere. NMR spectra were recorded in CDCl<sub>3</sub> for the PDMS macroinitiator and P3OTHPSt-b-PDMS-b-P3OTHPSt, and acetone- $d_6$  for P3HS-b-PDMS-b-P3OTHPSt, and acetone- $d_6$  for P3HS-b-PDMS-b-P3OTHPSt using a Bruker Avance-400 spectrometer. Both solvents contained no TMS as

the internal reference. Quantitative  ${}^{1}H$  NMR was performed with a 10 s relaxation delay. SAXS samples were prepared by the slow evaporation of THF solutions (5 wt % polymer in THF) and followed by annealing at 140 °C for 6 h under reduced pressure. The SAXS experiment was performed at the Dual Source and Environmental X-ray scattering (DEXS) facility operated by the Laboratory for Research on the Structure of Matter at the University of Pennsylvania. A Cu source ( $\lambda = 1.54 \text{ Å}$ ) was used and the sample-todetector distance was 1210 mm. Bulk films were sandwiched with Kapton support films to measure SAXS. The JEOL-F200 was used for transmission electron microscopy (TEM) measurements. For preparation of TEM samples, bulk films were embedded in epoxy and cured for 24 h (Buehler EpoxiCure). The samples embedded in epoxy were cross-sectioned with a thickness of ~50 nm using ultramicrotomy (Leica Ultracut S Ultramicrotome). The sectioned films were subsequently transferred to carbon-coated TEM grids. The TEM measurements were carried out without staining.

#### RESULTS AND DISCUSSION

**Synthesis of the Br-PDMS-Br Macroinitiator.** PDMS-based BCPs can be synthesized from commercially available PDMS homopolymers by further functionalization and extension of the chain ends. 51–53 As shown in Scheme 1,

Scheme 1. Synthetic Scheme of Bis(2-bromoisobutyrate)-Terminated PDMS Macroinitiator

$$HO \longrightarrow Si \longrightarrow Si \longrightarrow Si \longrightarrow OH + Br \longrightarrow OH$$

$$HO-PDMS-OH$$

$$THF$$

$$R.T.$$

$$Br \longrightarrow O \longrightarrow Si \longrightarrow Si \longrightarrow OH$$

$$Si \longrightarrow OH$$

$$R.T.$$

$$Br-PDMS-Br$$

$$n = 23, 47, 56, 90, 150$$

hydroxy-terminated PDMS was transformed into an ATRP macroinitiator by direct esterification with  $\alpha$ -bromoisobutyryl bromide. <sup>1</sup>H NMR spectra of HO-PDMS-OH and Br-PDMS-Br with peak assignments are shown in Figure 1. The methylene protons adjacent to the hydroxyl group shifted from 3.7 to 4.24 ppm following the conversion of the -OH to an ester group. Complete disappearance of the hydroxy peak at 2.15 ppm and the appearance of the dimethyl peak at 1.87 ppm confirmed the successful synthesis of Br-PDMS-Br. End-group analysis was used to determine the number-average molecular weight  $(M_n)$  as each peak is distinguishable. The HO-PDMS-OH starting material exhibited a broad unimodal SEC trace (inset in Figure 1) with a dispersity (D) of 1.96, whereas a narrower SEC trace was observed for Br-PDMS-Br with a dispersity of 1.57. This indicates that precipitation in methanol not only removed the impurities such as remaining  $\alpha$ bromoisobutyryl bromide from the esterification step but also fractionated the product by eliminating low molecular weight PDMS. In this work, five PDMS macroinitiators ranging in molecular weights from 1.7 to 11.1 kg/mol were used for chain extension to target triblocks with different lengths of the middle block.

Synthesis of the Triblock P3HS-b-PDMS-b-P3HS. The monomer 3OTHPSt was synthesized using previously

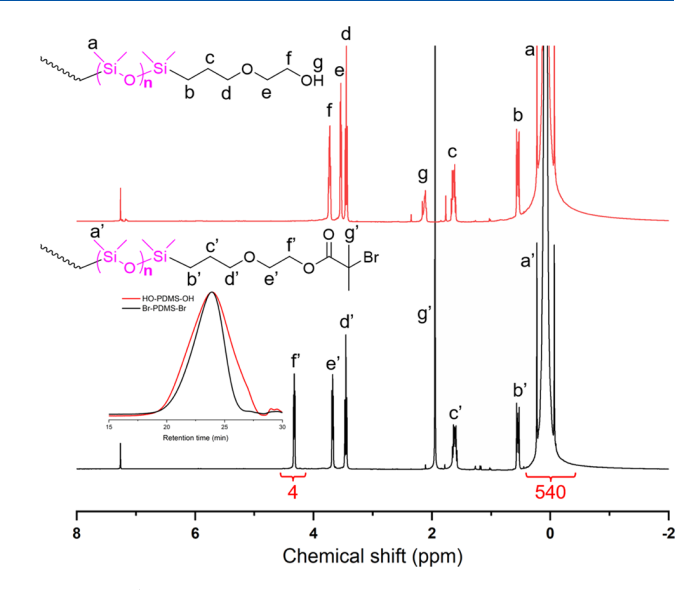


**Figure 1.** <sup>1</sup>H NMR spectra of HO-PDMS-OH (top) and Br-PDMS-Br (bottom) in CDCl<sub>3</sub>. The inset is the SEC traces for HO-PDMS-OH (red) and Br-PDMS-Br (black).

established methodology.<sup>29</sup> Prior to polymerization, the monomer was distilled over CaH<sub>2</sub> and stored in an Ar atmosphere. A series of P3HS-*b*-PDMS-*b*-P3HS were synthesized by ATRP (Scheme 2).

Five different Br-PDMS-Br macroinitiators were used to initiate the ATRP in a CuBr/TPMA catalyst system at 70 °C. To prevent side reactions or cross-linking caused by the -Br end group during further processing, a subsequent chain-end substitution from -Br to -H was carried out by adding excess tributyltin hydride to the system and extending the reaction for an additional 3 h. The solution was diluted and then poured into MeOH for precipitation, resulting in white powder as the final product. One of the advantages of this triblock is its powdery form that makes the purification and handling quite easy. In spite of the low glass transition temperature  $(T_{\sigma})$  of the PDMS block, the  $T_g$  of the P3OTHPSt block is relatively high, resulting in a powdery BCP.<sup>29</sup> The resultant polymers were then characterized by SEC and NMR. By changing the feed ratio of the Br-PDMS-Br macroinitiator and the 3HS monomer, 12 triblocks with various molecular weights and volume fractions were obtained (Table 1).

All SEC traces (Figure 2) were symmetric, indicating a well-controlled polymerization with dispersities ranging from 1.10 to 1.26. The <sup>1</sup>H spectra in Figure 3 (red) show all the characteristic peaks of THP at 5.3, 3.8, and 3.5 ppm, aromatic protons at 7.15–5.92 ppm, and the PDMS protons at 0 ppm, confirming the successful incorporation of P3OTHPSt. The molecular weights and volume fractions were determined by fixing the integration of the dimethylsiloxane protons obtained from the PDMS macroinitiator spectra and comparing it with the integration of the aromatic protons. <sup>29</sup>Si NMR showed a sharp peak at –22 ppm attributed to the O–Si–O of PDMS (Figure S2), confirming that the PDMS block remained intact.

To achieve the target P3HS-*b*-PDMS-*b*-P3HS triblock, the THP group was then deprotected using catalytic amounts of aqueous HCl solution. To prevent the potential hydrolysis of PDMS in the acidic solution, only a catalytic amount of HCl was used and the reaction time was optimized to 3 h at room temperature. The quantitative removal of the THP protecting groups was confirmed from the THP NMR spectra

# Scheme 2. Synthetic Scheme of P3HS-b-PDMS-b-P3HS Triblocks by ATRP

$$Br + O O \bigcirc_3 Si \bigcirc_3 S$$

Table 1. Molecular Characterization of P3HS-b-PDMS-b-P3HS

no.	sample	$M_{ m n,tol} \ ({ m kg/mol})^a$	$D^{b}$	$f_{\mathrm{P3HS}}^{c}$	$\begin{array}{c} \text{morphology} \\ (L_0)^{\vec{d}} \end{array}$
S1	1.7k-1.7k-1.7k	5.1	1.13	0.64	Dis
S2	1.4k-3.5k-1.4k	6.3	1.12	0.40	Lam (9.3 nm)
S3	1.2k-4.1k-1.2k	6.5	1.14	0.33	Lam (9.7 nm)
S4	1.8k-3.5k-1.8k	7.1	1.10	0.47	Lam (10.4 nm)
S5	1.9k-6.7k-1.9k	10.5	1.27	0.33	Lam (15.2 nm)
S6	3.7k-6.7k-3.7k	14.1	1.13	0.49	Cyl (29.0 nm)
<b>S</b> 7	5.4k-6.7k-5.4k	17.5	1.20	0.58	Cyl (26.9 nm)
S8	4.8k-11.1k-4.8k	20.7	1.21	0.42	Cyl (31.8 nm)
S9	7.1k-6.7k-7.1k	20.9	1.21	0.65	Cyl (29.7 nm)
S10	6.5k-11.1k-6.5k	24.1	1.19	0.49	Cyl (40.3 nm)
S11	6.8k-11.1k-6.8k	24.7	1.26	0.51	Cyl (40.8 nm)
S12	15.5k-6.7k-15.5k	37.7	1.19	0.80	Cyl

"Determined by quantitative <sup>1</sup>H NMR. <sup>b</sup>Determined by SEC using a polystyrene standard. <sup>c</sup>Determined using the homopolymer density:  $\rho(\text{P3HS}) = 1.15 \text{ g/cm}^3 \text{ and } \rho(\text{PDMS}) = 0.96 \text{ g/cm}^3.$  <sup>d</sup>Determined by SAXS measurement at room temperature; dimensions are calculated using  $L_0 = 2\pi/q^*$  and  $L_0 = 4\pi/\sqrt{3}\,q^*$  for lamellar and cylindrical morphology, respectively.

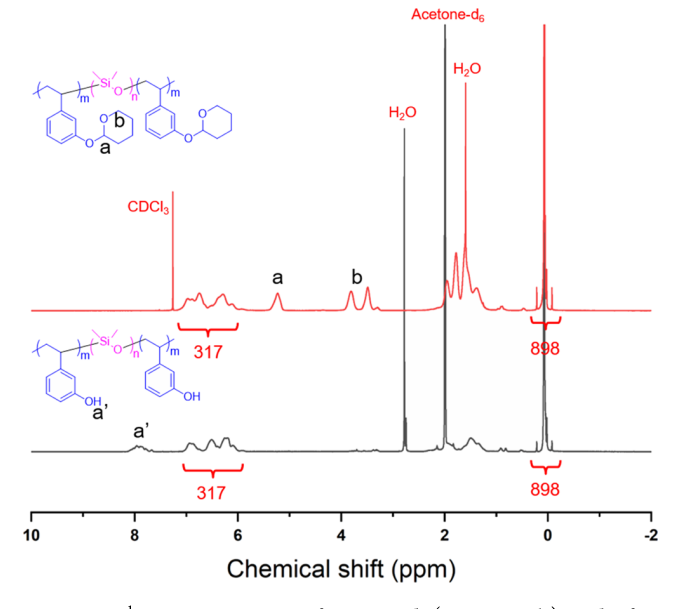


**Figure 3.**  $^{1}$ H NMR spectra of protected (top, CDCl<sub>3</sub>) and after deprotection (bottom, acetone- $d_6$ ) with a catalytic amount of HCl.

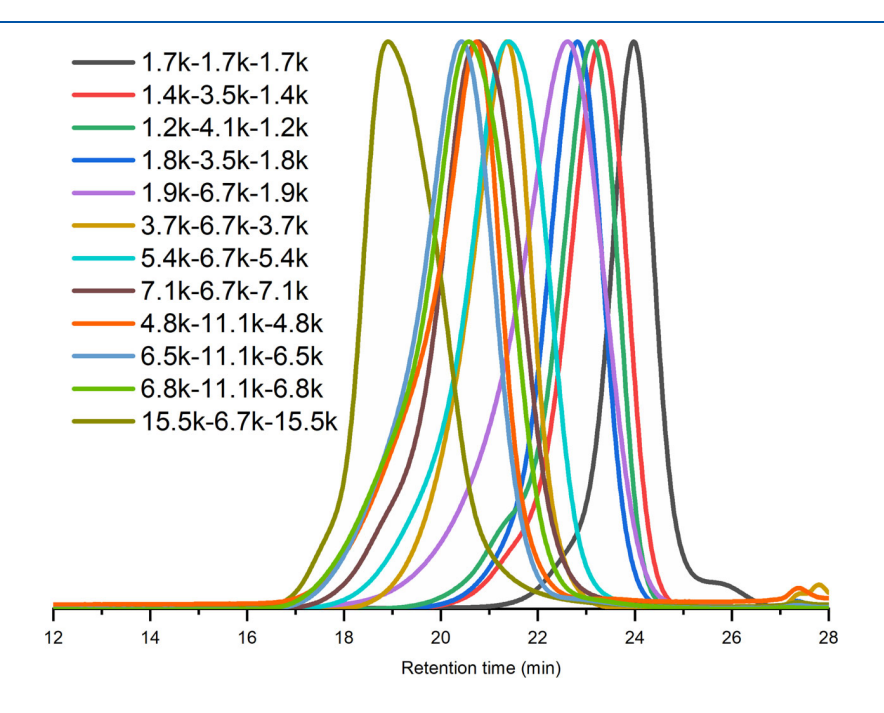
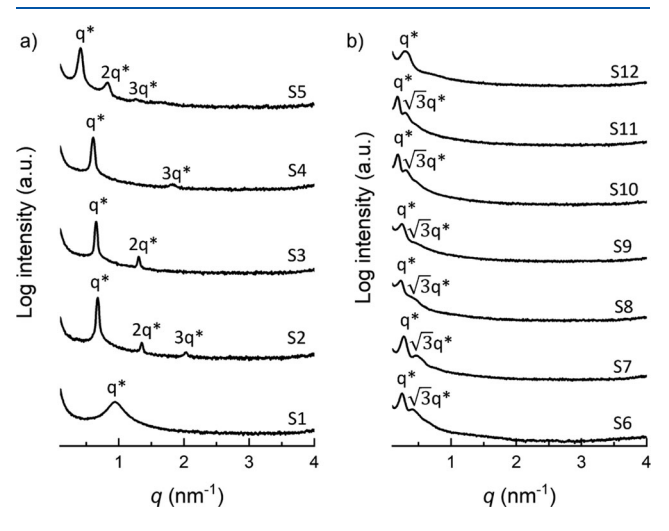


Figure 2. SEC chromatograms for P3OTHPSt-b-PDMS-b-P3OTHPSt triblocks.

(black line in Figure 3) by the appearance of the phenolic proton peak around 8 ppm as well as the disappearance of peaks at 5.3, 3.8, and 3.5 ppm. The presence of the large singlet at 0 ppm both before and after deprotection, as well as the constant integration ratio of the aromatic peaks from the P3HS to those from the PDMS before and after deprotection, confirmed that the PDMS block remained intact through the deprotection step.

Thermogravimetric analysis (TGA) was used to study the THP thermal deprotection and the thermal stability of the triblocks. TGA for the protected triblocks showed a two-step weight loss, corresponding to the loss of THP groups at 190 °C and the polymer backbone decomposition at 355 °C (Figure S3). In contrast, TGA for the deprotected P3HS-b-PDMS-b-P3HS showed a clean one-step degradation of the polymer backbone at 355 °C. In our earlier studies on the diblock poly(3-(2-tetrahydropyranyloxy)styrene)-b-poly(tert-butylstyrene) (P3OTHPSt-b-PtBuSt), thermal deprotection of the THP group was exploited to induce self-assembly in thin films by thermal annealing above 160 °C, while benefitting from the lower  $T_g$  of P3OTHPSt compared to P3HS. <sup>29</sup> For the triblocks, similar thermal deprotection-induced self-assembly is potentially feasible with a suitable surface neutral layer.

Bulk Self-Assembly of P3HS-b-PDMS-b-P3HS. Lamel-lae-Forming Compositions. Bulk self-assembly behavior of P3HS-b-PDMS-b-P3HS was studied by SAXS and TEM. All samples were prepared by thermal annealing of the THF-casted triblock films at 140 °C for 6 h. The SAXS pattern of the lowest molecular weight triblock S1 (1.7k-1.7k) showed a broad principal peak with no higher order peaks, indicating a disordered morphology (Figure 4a). As the



**Figure 4.** 1D SAXS profiles of (a) lamellar-forming and (b) cylinder-forming P3HS-*b*-PDMS-*b*-P3HS triblocks.

molecular weight increases, for the triblock S2 (1.4k-3.5k-1.4k), a distinct first-order peak and additional peaks at a  $q/q^*$  ratio of 1:2:3 (Figure 4a) confirmed a well-developed lamellar structure with a domain periodicity of 9.3 nm ( $L_0 = 2\pi/q^*$ ). The TEM image (Figure 5a) further confirmed the lamellar morphology. Hence, this triblock can be used to access sub-5 nm features. SAXS profiles of triblocks S2–S5 all display peaks with  $q:q^*$  with integral multiples. As expected, the domain periodicity increases as the molecular weight of the triblocks increases. The largest  $L_0$  obtained for the series synthesized in

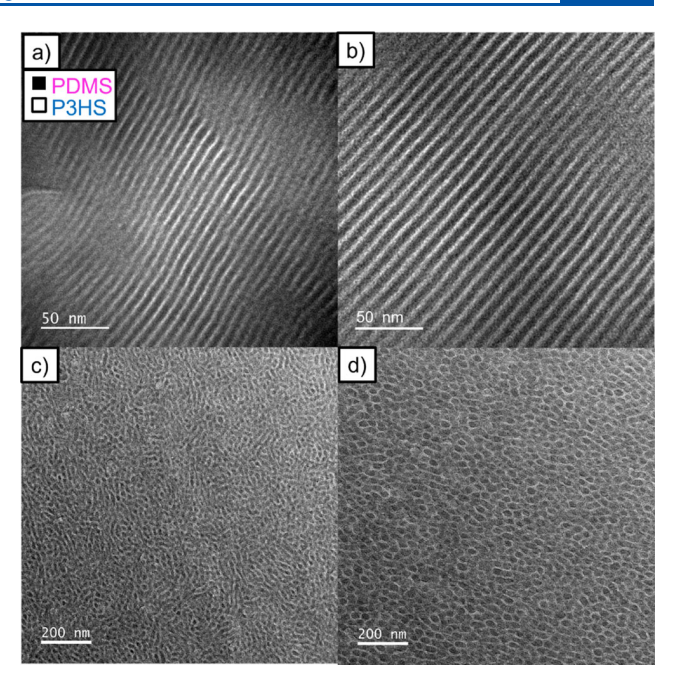


**Figure 5.** Representative TEM images of P3HS-*b*-PDMS-*b*-P3HS triblocks: (a) S2 1.4k-3.5k-1.4k, (b) S5 1.9k-6.7k-1.9k, (c) S7 5.4k-6.7 k-5.4k, and (d) S10 6.5k-11.1k-6.5k.

this work was 15.2 nm for S5 (1.9k-6.7k-1.9k), which was also confirmed by TEM (Figure 5b). The lamellar morphology for the S5 BCP persisted up to 250 °C, and no order—disorder transition was observed (Figure S4). All the temperature-dependent SAXS profiles in Figure S4 show a sharp primary peak and a secondary peak with a ratio of 1:2. The persistence of the lamellar morphology over the entire temperature range is a result of the high  $\chi$  nature of the triblock, and we surmise that the  $\chi N$  product remains in the strongly segregated regime throughout the temperatures considered.

Cylinder-Forming Compositions. Triblocks with higher P3HS volume fractions adopted a cylindrical morphology in which PDMS segments assemble to form cylinders within the P3HS matrix. SAXS patterns in Figure 4b show scattering peaks with a ratio of  $1:\sqrt{3}$ , characteristic of a cylindrical morphology. The increment in the interdomain spacing between neighboring cylinders ( $L_0 = 4\pi/\sqrt{3}q^*$ ) with increasing molecular weights of the BCP is apparent from the shift in the primary peaks to lower q values. As the molecular weight increased to 37.7 kg/mol in the S12 BCP, we did not observe any higher order peaks and instead observed only a broad peak. We did not observe any peak at a lower q value after further extending the sample-detector distance and annealing the sample at a higher temperature (160 °C, 6 h) (Figure S5). We performed the TEM measurement to confirm the morphology of the S12, and we found that the S12 exhibited less ordered cylinder morphology (Figure S6). We surmise that the poor ordering of the S12 is due to its highly symmetrical composition. Representative TEM images (Figure 5c,d) for S7 and S10 confirm the PDMS (dark region) cylindrical morphology in the P3HS (light region) matrix.<sup>5</sup>

Comparison between Diblocks and Triblocks. We previously reported the synthesis, bulk self-assembly, and phase diagram for P3HS-b-PDMS diblocks. <sup>15</sup> The strong segregation strength of this BCP was quantified by the high  $\chi$  of 0.39 at 150 °C, with  $\chi$  characterized by temperature-dependent

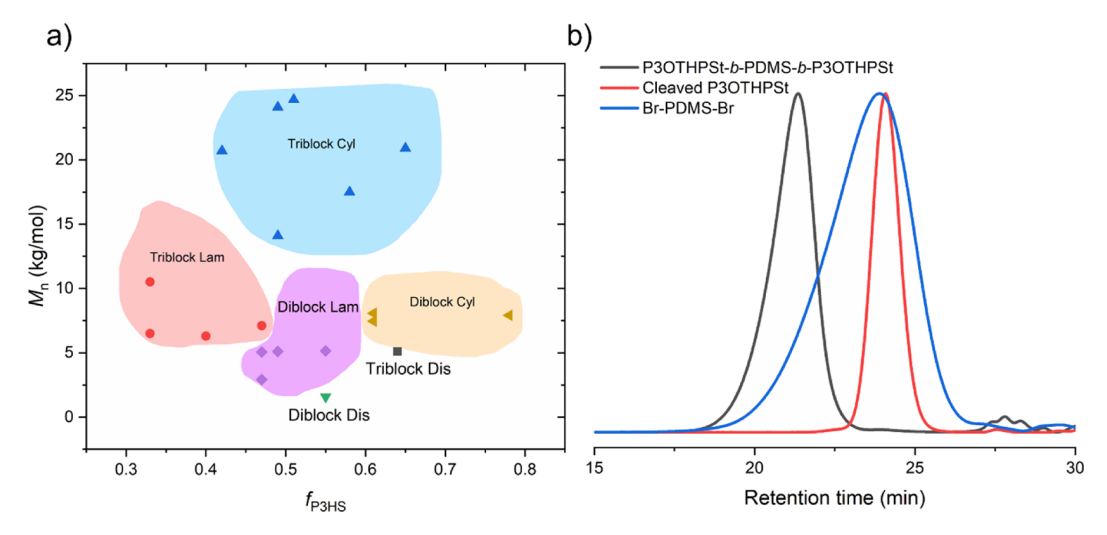


Figure 6. (a)  $M_n$  versus  $f_{P3HS}$  phase diagram for P3HS-b-PDMS-b-P3HS and P3HS-b-PDMS; (b) SEC traces for Br-PDMS-Br (blue), protected triblock P3OTHPSt-b-P3OTHPSt (black), and P3OTHPSt cleaved from the triblock after basic treatment (red).

correlation-hole scattering. The ABA (P3HS-b-PDMS-b-P3HS) triblocks should exhibit similar microphase separation behavior as their analogous AB diblocks. 58,59 The formation of sub-5 nm features from S2 (1.4k-3.5k-1.4k) in addition to the inaccessible order-disorder transition temperature are consistent with a large  $\chi$  parameter. The largest periodicity obtained from diblock was 18.6 nm from 4.1k-5.5k, whereas triblock 1.9k-6.7k-1.9k with larger molecular weight in the series resulted in a much smaller lamellar domain periodicity of 15.2 nm. When compared to the diblocks, it is known that triblocks can self-assemble into nanostructures with (a) similar dimensions as diblocks when  $N_{ABA} = 2N_{AB}^{44,45,47,60-63}$  and (b) smaller dimensions than that of the corresponding diblocks with the same molecular weights. The smallest lamellar periodicity achieved from P3HS-b-PDMS diblock was 7.4 nm for 1.5k-1.4k. Triblock 1.4k-3.5k-1.4k, on the other hand, provides the smallest lamellar periodicity of 9.4 nm, but the overall molecular weight (6.3 kg/mol) is much larger than that of diblock (2.9 kg/mol). A diblock with a comparable overall molecular weight of 3.8k-2.4k (6.2 kg/mol) formed a lamellar morphology with a larger periodicity of 11.5 nm.

The phase diagram of the diblock system mapped out in our earlier publication was in agreement with the theoretically predicted diagram, 8,15 whereas the triblock phase diagram shows a clear shift in the morphology window to lower P3HS volume fraction (Figure 6a). Such compositional shift is reminiscent of the dispersity-driven shift reported by Widin et al. 56 When ABA triblock consists of A block as a monodisperse hydrophilic segment and B block as a polydisperse hydrophobic segment, the real volume occupied by B block is smaller than expected based on the chemical composition alone. ABA triblocks with shorter B block desorb from the domain interfaces and act as an A-A dimer to enrich the A domain, and hence a shift toward lower  $f_A$  ( $f_{P3HS}$ ). Medium-long B chains pack at the domain interfaces to prevent chain stretching of longer B chains and the high configurational entropy of the system. 56,64,65 Hydrolysis of the triblock under a basic condition and subsequent SEC studies confirmed that this is indeed the case for our system (Figure 6b). P3OTHPSt cleaved from the triblock shows a narrow unimodal SEC trace with D = 1.05, confirming that the polymerization generated monodispersed end blocks with equal chain lengths. In

contrast, the PDMS macroinitiator has a broad distribution with a dispersity larger than 1.5. The same study was performed on diblock P3HS-b-PDMS synthesized by living anionic polymerization reported in our previous publication. Both diblock and cleaved P3OTHPSt exhibited a narrow dispersity (Figure S7). The compositional shift in the phase diagram for triblocks compared to diblocks is therefore attributed to the broad dispersity of the PDMS middle block. Lamellar domain dilation is typically observed when the block copolymer has polydisperse block in addition to a phase diagram shift. 65,66 Theoretical lamellar periodicities of S2-S5 were calculated based on the strong segregation theory and were compared with the dimensions obtained from SAXS (Table S2).67 The experimentally observed periodicities of S2-S5 are indeed dilated compared to the calculated values, which is consistent with previous theoretical and experimental work. 49,65,67,68

Preliminary thin-film assembly studies were performed using both diblock  $^{15}$  (4.1k-5.5k,  $L_0=18.6~\rm nm)$  and triblock (1.9k-6.7k-1.9k,  $L_0=15.2~\rm nm)$ . As shown in the SEM images and inset FFT (Figure S8), both lamellae-forming diblock and triblock were aligned perpendicularly to the substrate after solvent annealing under identical conditions. Qualitatively, from the images, the contrast between the diblock and triblock is stark. The triblock exhibited longer lamellar grains, whereas diblock formed relatively shorter lamellae. These results are promising as they confirm the advantages of triblock for thin-film assembly. Further optimization of the annealing conditions is ongoing along with pattern-transfer studies.

### SUMMARY

We have successfully synthesized and characterized a series of ultrahigh- $\chi$  ABA triblocks based on polyhydroxystyrene. Hydroxy-terminated PDMS of different lengths were functionalized to yield ATRP macroinitiators. A series of P3HS-b-PDMS-b-P3HS with various molecular weights and volume fractions of the two blocks were synthesized by ATRP and subsequently deprotected. The resultant triblocks showed well-developed lamellar and cylindrical morphologies. The smallest lamellar periodicity achieved was 9.3 nm, affording access to sub-5 nm feature size. We observed a composition-dependent shift in a morphological window toward lower P3HS volume

fraction, compared to the predicted phase diagram. By studying the dispersity of the P3HS end block and PDMS middle block, we conclude that this shift is attributable to the broader dispersity of the middle PDMS block, which complicates the packing at domain interfaces during self-assembly. Thin-film assembly of the triblocks and their comparison to their diblock counterparts and pattern transfer studies are ongoing.

# ASSOCIATED CONTENT

# **Solution** Supporting Information

The Supporting Information is available free of charge at https://pubs.acs.org/doi/10.1021/acs.macromol.1c01611.

SEC, <sup>29</sup>Si NMR, TGA, additional SAXS profiles, TEM images, and tables (PDF)

### AUTHOR INFORMATION

## **Corresponding Author**

Padma Gopalan — Department of Materials Science and Engineering, University of Wisconsin—Madison, Madison, Wisconsin 53706, United States; orcid.org/0000-0002-1955-640X; Email: pgopalan@wisc.edu

#### **Authors**

- Jian Sun Department of Materials Science and Engineering, University of Wisconsin–Madison, Madison, Wisconsin 53706, United States
- Changyeon Lee Department of Chemical and Biomolecular Engineering, University of Pennsylvania, Philadelphia, Pennsylvania 19104, United States
- Chinedum O. Osuji Department of Chemical and Biomolecular Engineering, University of Pennsylvania, Philadelphia, Pennsylvania 19104, United States; orcid.org/0000-0003-0261-3065

Complete contact information is available at: https://pubs.acs.org/10.1021/acs.macromol.1c01611

#### Notes

The authors declare no competing financial interest.

#### ACKNOWLEDGMENTS

This work was supported by the Wisconsin Alumni Research Foundation Accelerator program. J.S. acknowledges partial funding from NSF Award ID 2003891 for the phase behavior studies. P.G. and J.S. acknowledge the use of Wisconsin Centers for Nanoscale Technology, which is partially funded by NSF-MRSEC-1720415. C.L. and C.O.O. received support for the Dual Source and Environmental X-ray Scattering Facility at the University of Pennsylvania provided by the Laboratory for Structure and Matter, which is funded in part by NSF MRSEC 1720530.

## **■ REFERENCES**

- (1) Bates, C. M.; Maher, M. J.; Janes, D. W.; Ellison, C. J.; Willson, C. G. Block Copolymer Lithography. *Macromolecules* **2014**, *47*, 2–12.
- (2) Ruiz, R.; Kang, H.; Detcheverry, F. A.; Dobisz, E.; Kercher, D. S.; Albrecht, T. R.; de Pablo, J. J.; Nealey, P. F. Density Multiplication and Improved Lithography by Directed Block Copolymer Assembly. *Science* **2008**, *321*, 936.
- (3) Jo, A.; Joo, W.; Jin, W.-H.; Nam, H.; Kim, J. K. Ultrahigh-density phase-change data storage without the use of heating. *Nat. Nanotechnol.* **2009**, *4*, 727–731.

- (4) Fasolka, M. J.; Mayes, A. M. Block Copolymer Thin Films: Physics and Applications. *Annu. Rev. Mater. Res.* **2001**, *31*, 323–355.
- (5) Stoykovich, M. P.; Nealey, P. F. Block copolymers and conventional lithography. *Mater. Today* **2006**, *9*, 20–29.
- (6) Marencic, A. P.; Register, R. A. Controlling Order in Block Copolymer Thin Films for Nanopatterning Applications. *Annu. Rev. Chem. Biomol. Eng.* **2010**, *1*, 277–297.
- (7) Bates, F. S.; Fredrickson, G. H. Block Copolymer Thermodynamics: Theory and Experiment. *Annu. Rev. Phys. Chem.* **1990**, *41*, 525–557.
- (8) Leibler, L. Theory of Microphase Separation in Block Copolymers. *Macromolecules* **1980**, *13*, 1602–1617.
- (9) Semenov, A. N. Theory of block copolymer interfaces in the strong segregation limit. *Macromolecules* **1993**, *26*, 6617–6621.
- (10) Matsen, M. W.; Bates, F. S. Unifying Weak- and Strong-Segregation Block Copolymer Theories. *Macromolecules* **1996**, 29, 1091–1098.
- (11) Cushen, J. D.; Otsuka, I.; Bates, C. M.; Halila, S.; Fort, S.; Rochas, C.; Easley, J. A.; Rausch, E. L.; Thio, A.; Borsali, R.; Willson, C. G.; Ellison, C. J. Oligosaccharide/Silicon-Containing Block Copolymers with 5 nm Features for Lithographic Applications. *ACS Nano* 2012, 6, 3424–3433.
- (12) Katsuhara, S.; Mamiya, H.; Yamamoto, T.; Tajima, K.; Isono, T.; Satoh, T. Metallopolymer-block-oligosaccharide for sub-10 nm microphase separation. *Polym. Chem.* **2020**, *11*, 2995–3002.
- (13) Nowak, S. R.; Hwang, W.; Sita, L. R. Dynamic Sub-10-nm Nanostructured Ultrathin Films of Sugar—Polyolefin Conjugates Thermoresponsive at Physiological Temperatures. *J. Am. Chem. Soc.* **2017**, *139*, 5281–5284.
- (14) Mumtaz, M.; Takagi, Y.; Mamiya, H.; Tajima, K.; Bouilhac, C.; Isono, T.; Satoh, T.; Borsali, R. Sweet Pluronic poly(propylene oxide)-b-oligosaccharide block copolymer systems: Toward sub-4 nm thin-film nanopattern resolution. *Eur. Polym. J.* **2020**, *134*, 109831.
- (15) Azuma, K.; Sun, J.; Choo, Y.; Rokhlenko, Y.; Dwyer, J. H.; Schweitzer, B.; Hayakawa, T.; Osuji, C. O.; Gopalan, P. Self-Assembly of an Ultrahigh- $\chi$  Block Copolymer with Versatile Etch Selectivity. *Macromolecules* **2018**, *51*, 6460–6467.
- (16) Kwak, J.; Mishra, A. K.; Lee, J.; Lee, K. S.; Choi, C.; Maiti, S.; Kim, M.; Kim, J. K. Fabrication of Sub-3 nm Feature Size Based on Block Copolymer Self-Assembly for Next-Generation Nanolithography. *Macromolecules* **2017**, *50*, 6813–6818.
- (17) Yu, D. M.; Mapas, J. K. D.; Kim, H.; Choi, J.; Ribbe, A. E.; Rzayev, J.; Russell, T. P. Evaluation of the Interaction Parameter for Poly(solketal methacrylate)-block-polystyrene Copolymers. *Macromolecules* **2018**, *51*, 1031–1040.
- (18) Sinturel, C.; Bates, F. S.; Hillmyer, M. A. High  $\chi$ -Low N Block Polymers: How Far Can We Go? *ACS Macro Lett.* **2015**, *4*, 1044–1050.
- (19) Kim, S. O.; Solak, H. H.; Stoykovich, M. P.; Ferrier, N. J.; de Pablo, J. J.; Nealey, P. F. Epitaxial self-assembly of block copolymers on lithographically defined nanopatterned substrates. *Nature* **2003**, 424, 411–414.
- (20) Stoykovich, M. P.; Müller, M.; Kim, S. O.; Solak, H. H.; Edwards, E. W.; de Pablo, J. J.; Nealey, P. F. Directed Assembly of Block Copolymer Blends into Nonregular Device-Oriented Structures. *Science* **2005**, *308*, 1442.
- (21) Black, C. T. Polymer Self-Assembly as a Novel Extension to Optical Lithography. ACS Nano 2007, 1, 147–150.
- (22) Jung, Y. S.; Jung, W.; Tuller, H. L.; Ross, C. A. Nanowire Conductive Polymer Gas Sensor Patterned Using Self-Assembled Block Copolymer Lithography. *Nano Lett.* **2008**, *8*, 3776–3780.
- (23) Han, E.; Kim, M.; Gopalan, P. Chemical Patterns from Surface Grafted Resists for Directed Assembly of Block Copolymers. ACS Nano 2012, 6, 1823–1829.
- (24) Russell, T. P.; Hjelm, R. P.; Seeger, P. A. Temperature dependence of the interaction parameter of polystyrene and poly(methyl methacrylate). *Macromolecules* **1990**, 23, 890–893.
- (25) Choi, J. W.; Li, Z.; Black, C. T.; Sweat, D. P.; Wang, X.; Gopalan, P. Patterning at the 10 nanometer length scale using a

- strongly segregating block copolymer thin film and vapor phase infiltration of inorganic precursors. *Nanoscale* **2016**, *8*, 11595–11601.
- (26) Wan, L.; Ruiz, R.; Gao, H.; Patel, K. C.; Albrecht, T. R.; Yin, J.; Kim, J.; Cao, Y.; Lin, G. The Limits of Lamellae-Forming PS-b-PMMA Block Copolymers for Lithography. *ACS Nano* **2015**, 9, 7506–7514.
- (27) Sweat, D. P.; Yu, X.; Kim, M.; Gopalan, P. Synthesis of poly(4-hydroxystyrene)-based block copolymers containing acid-sensitive blocks by living anionic polymerization. *J. Polym. Sci., Part A: Polym. Chem.* **2014**, *52*, 1458–1468.
- (28) Sweat, D. P.; Kim, M.; Schmitt, A. K.; Perroni, D. V.; Fry, C. G.; Mahanthappa, M. K.; Gopalan, P. Phase Behavior of Poly(4-hydroxystyrene-block-styrene) Synthesized by Living Anionic Polymerization of an Acetal Protected Monomer. *Macromolecules* **2014**, 47, 6302–6310.
- (29) Kanimozhi, C.; Kim, M.; Larson, S. R.; Choi, J. W.; Choo, Y.; Sweat, D. P.; Osuji, C. O.; Gopalan, P. Isomeric Effect Enabled Thermally Driven Self-Assembly of Hydroxystyrene-Based Block Copolymers. ACS Macro Lett. 2016, 5, 833–838.
- (30) Ghoshal, T.; Ntaras, C.; O'Connell, J.; Shaw, M. T.; Holmes, J. D.; Avgeropoulos, A.; Morris, M. A. Fabrication of ultra-dense sub-10 nm in-plane Si nanowire arrays by using a novel block copolymer method: optical properties. *Nanoscale* **2016**, *8*, 2177–2187.
- (31) Son, J. G.; Gotrik, K. W.; Ross, C. A. High-Aspect-Ratio Perpendicular Orientation of PS-b-PDMS Thin Films under Solvent Annealing. *ACS Macro Lett.* **2012**, *1*, 1279–1284.
- (32) Peng, Q.; Tseng, Y.-C.; Darling, S. B.; Elam, J. W. Nanoscopic Patterned Materials with Tunable Dimensions via Atomic Layer Deposition on Block Copolymers. *Adv. Mater.* **2010**, *22*, 5129–5133.
- (33) Peng, Q.; Tseng, Y.-C.; Darling, S. B.; Elam, J. W. A Route to Nanoscopic Materials via Sequential Infiltration Synthesis on Block Copolymer Templates. *ACS Nano* **2011**, *5*, 4600–4606.
- (34) Moon, H.-S.; Kim, J. Y.; Jin, H. M.; Lee, W. J.; Choi, H. J.; Mun, J. H.; Choi, Y. J.; Cha, S. K.; Kwon, S. H.; Kim, S. O. Atomic Layer Deposition Assisted Pattern Multiplication of Block Copolymer Lithography for 5 nm Scale Nanopatterning. *Adv. Funct. Mater.* **2014**, 24, 4343–4348.
- (35) Ayothi, R.; Yi, Y.; Cao, H. B.; Yueh, W.; Putna, S.; Ober, C. K. Arylonium Photoacid Generators Containing Environmentally Compatible Aryloxyperfluoroalkanesulfonate Groups. *Chem. Mater.* **2007**, *19*, 1434–1444.
- (36) Hirao, A.; Loykulnant, S.; Ishizone, T. Recent advance in living anionic polymerization of functionalized styrene derivatives. *Prog. Polym. Sci.* **2002**, *27*, 1399–1471.
- (37) Vu, T.; Mahadevapuram, N.; Perera, G. M.; Stein, G. E. Controlling Domain Orientations in Thin Films of AB and ABA Block Copolymers. *Macromolecules* **2011**, *44*, 6121–6127.
- (38) Matsen, M. W. Architectural Effect on the Surface Tension of an ABA Triblock Copolymer Melt. *Macromolecules* **2010**, *43*, 1671–1674.
- (39) Khanna, V.; Cochran, E. W.; Hexemer, A.; Stein, G. E.; Fredrickson, G. H.; Kramer, E. J.; Li, X.; Wang, J.; Hahn, S. F. Effect of Chain Architecture and Surface Energies on the Ordering Behavior of Lamellar and Cylinder Forming Block Copolymers. *Macromolecules* **2006**, *39*, 9346–9356.
- (40) Lo, T.-Y.; Dehghan, A.; Georgopanos, P.; Avgeropoulos, A.; Shi, A.-C.; Ho, R.-M. Orienting Block Copolymer Thin Films via Entropy. *Macromolecules* **2016**, *49*, 624–633.
- (41) Jang, S.; Lee, K.; Moon, H. C.; Kwak, J.; Park, J.; Jeon, G.; Lee, W. B.; Kim, J. K. Vertical Orientation of Nanodomains on Versatile Substrates through Self-Neutralization Induced by Star-Shaped Block Copolymers. *Adv. Funct. Mater.* **2015**, *25*, 5414–5419.
- (42) Lu, K.-Y.; Lo, T.-Y.; Georgopanos, P.; Avgeropoulos, A.; Shi, A.-C.; Ho, R.-M. Orienting Silicon-Containing Block Copolymer Films with Perpendicular Cylinders via Entropy and Surface Plasma Treatment. *Macromolecules* **2017**, *50*, 9403–9410.
- (43) Park, S. Y.; Choi, C.; Lee, K. S.; Kim, E.; Ahn, S.; Lee, J.; Kim, J. K. Microdomain Orientation of Star-Shaped Block Copolymer Thin

- Film Depending on Molecular Weight. *Macromolecules* **2020**, 53, 3611–3618.
- (44) Xiong, S.; Wan, L.; Ishida, Y.; Chapuis, Y.-A.; Craig, G. S. W.; Ruiz, R.; Nealey, P. F. Directed Self-Assembly of Triblock Copolymer on Chemical Patterns for Sub-10-nm Nanofabrication via Solvent Annealing. *ACS Nano* **2016**, *10*, 7855–7865.
- (45) Lee, S.; Cheng, L.-C.; Gadelrab, K. R.; Ntetsikas, K.; Moschovas, D.; Yager, K. G.; Avgeropoulos, A.; Alexander-Katz, A.; Ross, C. A. Double-Layer Morphologies from a Silicon-Containing ABA Triblock Copolymer. *ACS Nano* **2018**, *12*, 6193–6202.
- (46) Pang, Y.; Jin, X.; Huang, G.; Wan, L.; Ji, S. Directed Self-Assembly of Styrene-Methyl Acrylate Block Copolymers with Sub-7 nm Features via Thermal Annealing. *Macromolecules* **2019**, *52*, 2987–2994.
- (47) Matsen, M. W.; Thompson, R. B. Equilibrium behavior of symmetric ABA triblock copolymer melts. *J. Chem. Phys.* **1999**, *111*, 7139–7146.
- (48) Matsen, M. W.; Schick, M. Lamellar phase of a symmetric triblock copolymer. *Macromolecules* **1994**, 27, 187–192.
- (49) Matsen, M. W. Comparison of A-block polydispersity effects on BAB triblock and AB diblock copolymer melts. *Eur. Phys. J. E* **2013**, 36. 44.
- (50) Ryu, C. Y.; Lee, M. S.; Hajduk, D. A.; Lodge, T. P. Structure and viscoelasticity of matched asymmetric diblock and triblock copolymers in the cylinder and sphere microstructures. *J. Polym. Sci., Part B: Polym. Phys.* **1997**, 35, 2811–2823.
- (51) Peng, H.; Cheng, S.; Feng, L.; Fan, Z. Synthesis of block copolymers from PDMS macroinitiators. *Polym. Int.* **2004**, *53*, 833–837.
- (52) Semsarzadeh, M. A.; Abdollahi, M. Atom transfer radical polymerization of styrene and methyl (meth)acrylates initiated with poly(dimethylsiloxane) macroinitiator: Synthesis and characterization of triblock copolymers. *J. Appl. Polym. Sci.* **2012**, *123*, 2423–2430.
- (53) Lopez-Oliva, A. P.; Warren, N. J.; Rajkumar, A.; Mykhaylyk, O. O.; Derry, M. J.; Doncom, K. E. B.; Rymaruk, M. J.; Armes, S. P. Polydimethylsiloxane-Based Diblock Copolymer Nano-objects Prepared in Nonpolar Media via RAFT-Mediated Polymerization-Induced Self-Assembly. *Macromolecules* **2015**, *48*, 3547–3555.
- (54) Griessbach, E. F. C.; Lehmann, R. G. Degradation of polydimethylsiloxane fluids in the environment a review. *Chemosphere* **1999**, 38, 1461–1468.
- (55) Sakamoto, N.; Hashimoto, T. Order-Disorder Transition of Low Molecular Weight Polystyrene-block-Polyisoprene. 1. SAXS Analysis of Two Characteristic Temperatures. *Macromolecules* 1995, 28, 6825–6834.
- (56) Widin, J. M.; Schmitt, A. K.; Schmitt, A. L.; Im, K.; Mahanthappa, M. K. Unexpected Consequences of Block Polydispersity on the Self-Assembly of ABA Triblock Copolymers. *J. Am. Chem. Soc.* **2012**, *134*, 3834–3844.
- (57) Barnes, A. M.; Du, Y.; Zhang, W.; Seifert, S.; Buratto, S. K.; Coughlin, E. B. Phosphonium-Containing Block Copolymer Anion Exchange Membranes: Effect of Quaternization Level on Bulk and Surface Morphologies at Hydrated and Dehydrated States. *Macromolecules* 2019, 52, 6097–6106.
- (58) Milner, S. T. Chain Architecture and Asymmetry in Copolymer Microphases. *Macromolecules* **1994**, *27*, 2333–2335.
- (59) Helfand, E.; Wasserman, Z. R. Block Copolymer Theory. 4. Narrow Interphase Approximation. *Macromolecules* **1976**, *9*, 879–888.
- (60) Mayes, A. M.; Olvera de la Cruz, M. Microphase separation in multiblock copolymer melts. *J. Chem. Phys.* **1989**, *91*, 7228–7235.
- (61) Ji, S.; Nagpal, U.; Liu, G.; Delcambre, S. P.; Müller, M.; de Pablo, J. J.; Nealey, P. F. Directed Assembly of Non-equilibrium ABA Triblock Copolymer Morphologies on Nanopatterned Substrates. *ACS Nano* **2012**, *6*, 5440–5448.
- (62) Mai, S.-M.; Mingvanish, W.; Turner, S. C.; Chaibundit, C.; Fairclough, J. P. A.; Heatley, F.; Matsen, M. W.; Ryan, A. J.; Booth, C. Microphase-Separation Behavior of Triblock Copolymer Melts. Comparison with Diblock Copolymer Melts. *Macromolecules* **2000**, 33, 5124–5130.

- (63) Shen, Z.; Chen, J. L.; Vernadskaia, V.; Ertem, S. P.; Mahanthappa, M. K.; Hillmyer, M. A.; Reineke, T. M.; Lodge, T. P.; Siepmann, J. I. From Order to Disorder: Computational Design of Triblock Amphiphiles with 1 nm Domains. *J. Am. Chem. Soc.* **2020**, 142, 9352–9362.
- (64) Beardsley, T. M.; Matsen, M. W. Monte Carlo Phase Diagram for a Polydisperse Diblock Copolymer Melt. *Macromolecules* **2011**, *44*, 6209–6219.
- (65) Schmitt, A. L.; Mahanthappa, M. K. Polydispersity-driven shift in the lamellar mesophase composition window of PEO-PB-PEO triblock copolymers. *Soft Matter* **2012**, *8*, 2294–2303.
- (66) Lynd, N. A.; Hillmyer, M. A. Influence of Polydispersity on the Self-Assembly of Diblock Copolymers. *Macromolecules* **2005**, *38*, 8803–8810.
- (67) Ruzette, A.-V.; Tencé-Girault, S.; Leibler, L.; Chauvin, F.; Bertin, D.; Guerret, O.; Gérard, P. Molecular Disorder and Mesoscopic Order in Polydisperse Acrylic Block Copolymers Prepared by Controlled Radical Polymerization. *Macromolecules* **2006**, 39, 5804–5814.
- (68) Matsen, M. W. Effect of large degrees of polydispersity on strongly segregated block copolymers. *Eur. Phys. J. E: Soft Matter Biol. Phys.* **2006**, 21, 199–207.